Journal of Solid State Chemistry 187 (2012) 159–164

Contents lists available at SciVerse ScienceDirect

Journal of Solid State Chemistry

journal homepage: www.elsevier.com/locate/jssc

Exploration on anion ordering, optical properties and electronic structure in $K_3WO_3F_3$ elpasolite

V.V. Atuchin [a], L.I. Isaenko [b], V.G. Kesler [c], Z.S. Lin [d,*], M.S. Molokeev [e], A.P. Yelisseyev [b], S.A. Zhurkov [b]

[a] Laboratory of Optical Materials and Structures, Institute of Semiconductor Physics, SB RAS, Novosibirsk 630090, Russia
[b] Laboratory of Crystal Growth, Institute of Geology and Mineralogy, SB RAS, Novosibirsk 630090, Russia
[c] Laboratory of Physical Principles for Integrated Microelectronics, Institute of Semiconductor Physics, Novosibirsk 630090, Russia
[d] Technical Institute of Physics and Chemistry, Chinese Academy of Sciences, P.O. Box 2711, Beijing 100190, China
[e] Laboratory of Crystal Physics, Institute of Physics, SB RAS, Krasnoyarsk 660036, Russia

ARTICLE INFO

Article history:
Received 17 August 2011
Received in revised form
7 December 2011
Accepted 26 December 2011
Available online 12 January 2012

Keywords:
Oxyfluorotungstate
Structure
Nonlinear optical crystals
Electronic and optical properties
First-principles calculations

ABSTRACT

Room-temperature modification of potassium oxyfluorotungstate, G2-$K_3WO_3F_3$, has been prepared by low-temperature chemical route and single crystal growth. Wide optical transparency range of 0.3–9.4 μm and forbidden band gap E_g=4.32 eV have been obtained for G2-$K_3WO_3F_3$ crystal. Meanwhile, its electronic structure has been calculated with the first-principles calculations. The good agreement between the theorectical and experimental results have been achieved. Furthermore, G2-$K_3WO_3F_3$ is predicted to possess the relatively large nonlinear optical coefficients.

1. Introduction

Complex metal oxyfluorides are attractive compounds for creation new noncentrosymmetric crystals because the strong distortion of metal-(O,F) polyhedra in crystal lattice is achieved due to different ionicity of metal-O and metal-F bonds. This strategy is particularly successful in design of new oxyfluoroborates containing boron-(O,F) polyhedra and possessing interesting nonlinear optical properties and wide transparency range [1–4]. Effects of mixed anion sublattice, however, are considered for a long time for a suite of transition metals compounds with $[MO_{6-x}F_x]$ (M=W, Mo, Nb, Ti) groups [5–11]. From geometrical point of view, the strongest distortion of separated $[MO_{6-x}F_x]$ octahedron is achieved for x=3 and such polar structural group seems to be optimal for generation of low-symmetry complex compounds [6]. These distorted octahedrons can be stacked without the center of inversion in the crystal lattice if long range ordering condition is fulfilled. Indeed, several noncentrosymmetric inorganic crystals containing ordered $[MO_3F_3]$ (M=Mo, W) groups were found at enough low temperatures [6,10,12–16].

Oxyfluorides $A_2BMO_3F_3$ (A, B=Na, K, Rb, Cs, Tl, NH_4; M=Mo, W) show similar structural, ferroelectric and ferroelastic properties within the certain temperature intervals [10,13,14,17,18]. Cubic paraelectric phase G0 with elpasolite-type parent structure in space group *Fm*-3*m* has been found for $A_2BMO_3F_3$ compounds at high temperature range $T > T_1$ [8,9,16,18–21]. Complete disorder in anion positions is a principal characteristic of this state. At low temperatures $T \le T_1$ partial anion ordering results in subsequent phase transitions with formation of low-symmetry phases Gi. For many $A_2BMO_3F_3$ compounds the structural transitions are accompanied by noticeable dielectric and caloric effects [10,13,14,17,18,20,22–24]. Piezoelectric Gi-phases were found for several cation compositions but detailed information on physical properties of the compounds is practically absent in literature for lack of oxyfluoride single crystals with size and quality needed for the measurements. To our best knowledge, only the few-hundred-μm-size $Rb_2KMoO_3F_3$, $K_3MoO_3F_3$, $(Ag_3MoO_3F_3)(Ag_3MoO_4)Cl$, $Ag_3MoO_3F_3$ and $Ag_3VO_2F_4$ crystals were grown up to now because of the great technological difficulty to grow oxyfluoride crystals with reasonable size [19,25,26].

For the representative compound $K_3WO_3F_3$ from $A_2BMO_3F_3$ family, the transitions of ferroelectric G0↔G1 and ferroelastic G1↔G2 character were defined to be at T_1=452 K and T_2=414 K, respectively [10,14,17,27]. The entropy variation under the transition was found to be $\Delta S_1 = R\ln(1.68)$ and $\Delta S_2 = R\ln(1.42)$ [10,14]. Crystal structures of G1-$K_3WO_3F_3$ and G2-$K_3WO_3F_3$ modifications were refined by powder methods in space groups *I*4*mm* and *Cm*, respectively, with evident indication of O^{2-} and F^- ion ordering at anion positions [15,16]. Vibrational spectra and

* Corresponding author. Fax: +86 10 82543709.
E-mail address: zslin@mail.ipc.ac.cn (Z.S. Lin).

0022-4596/$ - see front matter © 2012 Elsevier Inc. All rights reserved.
doi:10.1016/j.jssc.2011.12.037

electronic structure of G2-$K_3WO_3F_3$ were examined with Raman, IR and X-ray photoelectron spectroscopy (XPS) for powder samples [27,28]. Noticeable variation of W–O mean bond ionicity in G2-$K_3WO_3F_3$, as it seems due to presence of W–F bonds, was found by XPS in reference to that in pure tungstates [29]. However, other properties of $K_3WO_3F_3$ remain to be unclear. Present study is aimed to grow the crystals of low-temperature ferroelectric G2-$K_3WO_3F_3$ polymorph. Optical properties and electronic structure are then evaluated comparatively by experimental and theoretical methods.

2. Experimental

2.1. Chemical synthesis and crystal growth

Powder sample of $K_3WO_3F_3$ was fabricated by low-temperature chemical synthesis from water-based solutions. As starting reagents the KF (99.9%) and K_2WO_4 (99.5%) were used. At a first step a solution of potassium fluoride in hydrofluoric acid was prepared. After this, a solution of potassium tungstate in distilled water was carried out. Then, these two solutions were mixed with precautions because the reaction is active and with heating. As a result of reaction, white precipitate was separated out of mother solution. After drying a white-colored powder product was formed.

Water-free KF and WO_3 were used as starting materials to produce $K_3WO_3F_3$ single crystals. Water-free KF was obtained by evaporating $KF \times 2H_2O$ with adding of concentrated etching acid. NH_4F was added to dry the remainder and resulting substance was heated to 300 °C in a teflon crucible to remove the remained water and alkali according the following reaction:

$$KOH + NH_4F = KF + H_2O\uparrow + NH_3\uparrow$$

The obtained substance was heated to 500 °C in closed Pt crucible in presence of teflon which was used as a fluorine agent. Then substance was grinded in a mortar, mixed with teflon boring and placed into a Pt crucible with a cover. The crucible was heated to 900 °C, the temperature above KF melting temperature, in a flow of dry nitrogen. Before using, WO_3 was heated to 700 °C in a Pt crucible. The synthesis of $K_3WO_3F_3$ compound was carried out from a charge of stoichiometric composition:

$$3KF + WO_3 = K_3WO_3F_3$$

The mixture was grinded in a mortar and placed into a Pt ampule. The ampule was then located on a chamotte support inside a growth furnace and covered with a Pt cover, under which dry nitrogen was delivered during the whole growth experiment. The furnace was heated to 980 °C at a 30 °C/h rate. Then furnace was kept at this temperature during 6 h and afterwards temperature was lowered during 2 day at a rate of 1 °C/h. The obtained crystal was cooled at a rate of 30 °C/h. In a result the cm-size $K_3WO_3F_3$ single crystals were formed by this technique as shown in Fig. 1. The crystals are transparent and enough large for optical measurements. It should be pointed that presently crystal growth technology is well developed only for nonlinear optical oxyfluoroborates. As to other oxyfluorides, typically powder samples formed by chemical synthesis are used for physical properties observation [8,10,13–18,20,23]. For several oxyfluorides tiny single crystals were fabricated with dimensions enough for single crystal structure determination [12,19,21,26]. To our best knowledge, up to now preparation of optical quality mm-size crystals was achieved only for $K_3MoO_3F_3$, $(NH_4)_2WO_2F_4$ and $(NH_4)_2NbOF_5$ compounds [25,30,31]. The technology developed in present study for creation of large $K_3WO_3F_3$ is universal and can be applied for other oxyfluorides.

Fig. 1. Photo of $K_3WO_3F_3$ single crystal on the background of Times Roman font 12.

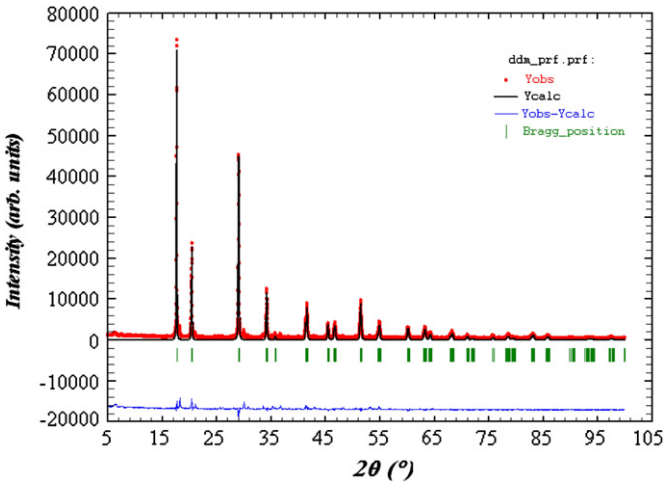

Fig. 2. XRD analysis of $K_3WO_3F_3$ crystal at room temperature. *Cm* space group.

Phase composition of grown $K_3WO_3F_3$ crystal at room temperature was evaluated with XRD analysis. The results of the XRD analysis are shown in Fig. 2. Presence of pure monoclinic G2-$K_2WO_3F_3$, space group *Cm*, modification was found with structural parameters $a=8.7459(2)$ Å, $b=8.6930(4)$ Å, $c=6.1650(3)$ Å, $\beta=135.178(2)^\circ$.

2.2. Structure determination

Structure determination of G0, G1 and G2 polymorph modifications of $K_3WO_3F_3$ has been produced with Rietveld analysis for powder sample prepared by chemical synthesis. The powder X-ray diffraction patterns were collected at 298, 433 and 513 K with a Bruker D8 ADVANCE diffractometer in the Bragg-Brentano geometry and linear Vantec detector [16]. Operating parameters were: CuK_α radiation, tube voltage 40 kV, tube current 40 mA, step size 0.016°, counting time 1 s per step. The data were collected over the range 5–110°. Peak positions were determined with the program EVA, available in the PC software package DIFFRAC-PLUS supplied from Bruker. X-ray patterns of the title compound were indexed using the program McMaille [33]. The details of the analysis (e.g., R-factors) for the diffraction data sets

Table 1
Fractional coordinates, occupancies (p) and isotropic atomic displacement parameters (B_i) for $K_3WO_3F_3$.

Atom	p	Wyckoff positions	Number of atoms in unit cell	X	Y	Z	$B_{iso.}$,Å^2
Fm-3, G0							
W	1.0	4a	4*1.0=4	0	0	0	3.90(4)
K1	1.0	4b	4*1.0=4	1/2	1/2	1/2	6.9(1)
K2	1.0	8c	8*1.0=8	1/4	1/4	1/4	5.8(1)
F	0.5	24e	24*0.5=12	0.219(2)	0	0	4.3(3)
O	0.125	96j	96*0.125=12	0.192(3)	0.092(2)	0	4.4(7)
I4 mm, G1							
W	1.0	2a	2*1.0=2	1/2	1/2	1/2	3.82(4)
K1	1.0	2a	2*1.0=2	0	0	0.497(8)	9.5(3)
K2	1.0	4b	4*1.0=4	1/2	0	0.262(2)	5.2(2)
F1	0.5	8c	8*0.5=4	0.277(3)	0.277(3)	0.526(4)	4.1(6)
F2	1	2a	2*1.0=2	0	0	0.217(2)	1.0(4)
O1	0.25	16e	16*0.25=4	0.228(5)	0.606(5)	0.560(4)	4.1(6)
O2	0.25	8c	8*0.25=2	0.110(6)	0.110(6)	0.822(5)	3(1)
Cm, G2							
W	1.0	2a	2*1.0=2	0	0	0	4.5(1)
K1	1.0	2a	2*1.0=2	−0.06(1)	0.5	−0.078(8)	7.1(9)
K2	1.0	4b	4*1.0=4	0.006(3)	0.719(2)	0.470(5)	1.9(4)
F1	1.0	2a	2*1.0=2	0.275(7)	0	0.07(1)	2.0(1)
F2	1.0	2a	2*1.0=2	0.73(1)	1/2	0.46(1)	2.0(1)
F3	0.5	4b	4*0.5=2	0.04(1)	0.204(7)	0.14(1)	2.0(1)
O1	1.0	2a	2*1.0=2	0.80(1)	0	0.60(1)	2.0(1)
O2	1.0	2a	2*1.0=2	0.81(1)	0	0.00(1)	2.0(1)
O3	0.5	4b	4*0.5=2	0.04(1)	0.204(7)	0.14(1)	2.0(1)

collected at the three temperatures were reported in Ref. [16], in which the results have been discussed using the group-theoretical analysis of the complete order parameter condensate and taking into account the critical and noncritical atomic displacements. In present study, however, the structural parameters of known $K_3WO_3F_3$ modifications are completed and corrected. Final structural parameters of G0-, G1- and G2-$K_3WO_3F_3$ modifications are shown in Table 1.

2.3. Optical measurements

Absorption/luminescence spectra for $K_3WO_3F_3$ were measured for the plates with thickness of 1.8 mm. The plates were cut and polished without crystallographic orientation control. Optical measurements were produced using a UV-2501PC Shimadzu spectrometer in the UV to near IR region and a Fourier transform spectrometer Infralum FT-801 in the mid IR. Spectra in the short wavelength range were measured using a metal cryostat with silica windows. Absorption coefficients were calculated from transmission measurements in the transparency region by use of the following formula [32]:

$$T=(1-R)^2e^{-\alpha d}/(1-R^2e^{-2\alpha d}) \quad (1)$$

where α is the absorption coefficient (cm^{-1}), d is the sample thickness (cm) and R is the power reflection coefficient per surface. Maximum transmission level allows to estimate roughly the refraction index n and reflection index R as well as to calculate α. An attempt has been made to determine the dominant mechanism of band-to-band electronic transitions. The kind of transition can be defined from the functional relationship between absorption α and the photon energy $h\nu$ [32].

Thus, for direct-allowed and indirect-allowed transitions the relations $\alpha h\nu \propto (h\nu - E_g)^{1/2}$ and $\alpha h\nu \propto (h\nu - E_g)^2$ are fullfilled, respectively. The estimations were carried out for a 0.3 mm thick $K_3WO_3F_3$ plate. The band gap values E_g were estimated by extrapolating the linear part of the $(\alpha h\nu)^2$ versus $h\nu$ or $(\alpha h\nu)^{1/2}$ versus $h\nu$ curves to $\alpha(h\nu)=0$.

2.4. Valence band structure by XPS

Observation of valence band structure of $K_3WO_3F_3$ was produced by using surface analysis center SSC (Riber) with X-ray photoelectron spectroscopy (XPS) method for powder sample prepared by chemical synthesis. The nonmonochromatic AlK_α radiation (1486.6 eV) with the power source of 300 W was used for the excitation of photoemission. The energy resolution of the instrument was chosen to be 0.7 eV. Under the conditions the observed full width at half maximum (FWHM) of the Au $4f_{7/2}$ line was 1.31 eV. The binding energy (BE) scale was calibrated in reference to the Cu $3p_{3/2}$ (75.1 eV) and Cu $2p_{3/2}$ (932.7 eV) lines, assuring an accuracy of 0.1 eV in any peak energy position determination. Photoelectron energy drift due to charging effects was taken into account in reference to the position of the C 1s (284.6 eV) line generated by adventitious carbon present on the surface of the powder as-inserted into the vacuum chamber.

3. Computational method

In this work, the electronic structures and optical properties for the G2-$K_3WO_3F_3$ phase are theoretically studied. The first-principles calculations were performed using the plane-wave pseudopotential method [34] implemented in the CASTEP package [35]. Ultrasoft pseudopotentials [36] are used with the 3s, 3p and 4s electrons for potassium and the 5s, 5p, 5d and 6s electrons for tungsten treated as valence electrons. For oxygen and fluorine, 1s electrons are chosen as the core electrons. Generalized-gradient approximation (GGA) using the Perdew, Burke, and Ernzerhof (PBE) [37] exchange-correlation functional has been used. The kinetic energy cutoff is set as 600 eV. Monkhorst–Pack k point meshes [38] with a density of $(5\times5\times6)$ points in the Brillouin zone of the primitive cell are used. Since the position occupancies for some oxygen and fluorine atom are not unity, the virtual crystal approximation (VCA) [39] are adopted to take into account the weight average of the potential of each atomic species at the position.

4. Results and discussion

The transmission spectra recorded at 300 K for 1.8 mm thick G2-$K_3WO_3F_3$ crystal plate is given in Fig. 3(a). The transparency range is from 0.3 to 9.4 μm at the 5% transmission level. Transmission grows quickly as wavelength increases but there is a kink near $\lambda \sim 0.35$ μm after which transmission grows much slower till $\lambda \sim 4$ μm. There is a suite of intensive absorption bands in the range $\lambda = 5.0$–6.5 μm with a maximum at 5.8 μm. The losses in the $\lambda \sim 0.35$–4 μm range are due to light scattering. The intensity of nonresonant Rayleigh scattering is $\sigma \sim \lambda^{-4} r^6 (\varepsilon - \varepsilon_0)$, where r is the size of scattering particles (inclusions in our case) with $r \ll \lambda$, ε and ε_0 are the dielectric permittivity of scattering substance and the surrounding medium (crystal), so the scattering intensity is high at shorter wavelengths and decreases gradually into the IR spectral region. The intense absorption near $\lambda \sim 6$ μm is likely due to deformation vibrations of the residual H_2O individual molecules which are tied by stronger hydrogen bonds [40]. These intense bands were also observed in mica, e.g., in phlogopite, muscovite: they are associated with the water molecules adsorbed on the surface and between the structural layers [41]. In addition, there may be some input of the second harmonic from intense bands near 825 (12.12 μm) and 925 cm^{-1} (10.81 μm), which are active both in IR absorption and Raman spectra. Both bands are resulted from the stretching vibrations of the W–O bond of the $[WO_3F_3]^{3-}$ ionic groups [27]. Well-pronounced bands at $\lambda \sim 7.75$ (1290 cm^{-1}) and 8.38 μm (1193 cm^{-1}), therefore, may be the sums of the stretching vibrations of the W–O bond and the stretching vibrations of the W–F bond in the $[WO_3F_3]^{3-}$ ionic groups: $\sim 925 + 375$ cm^{-1} and $\sim 825 + 375$ cm^{-1}, respectively [27]. Maximum transmission in the range from 4 to 7.5 μm is ~82%, except the band at $\lambda \sim 5.8$ μm. Rough estimation shows that at zero absorption the reflection coefficients are ~9.5% and 18% for single and multiple reflections, respectively, corresponding to the refraction indices as high as $n \sim 1.9$. We believe that both light scattering and absorption in the $K_3WO_3F_3$ transparency range from 0.35 to 7.0 μm can be removed and expected transmission spectrum of a high quality crystal is shown by a dotted line in Fig. 3(a). We established that fundamental absorption edge rectifies in the coordinates $(\alpha h\nu)^2 = f(h\nu)$ (Fig. 3(b)) and this indicates that direct allowed electronic transitions determine the absorption edge shape. The cross points between the approximation straight line and abscissa axis $(\alpha h\nu) = 0$ give the bandgap value E_g for G2-$K_3WO_3F_3$ polymorph, which is 4.413 and 4.315 eV at 80 and 300 K, respectively. Such magnitude of E_g shift (~0.1 eV) with temperature variation is typical for oxides [42].

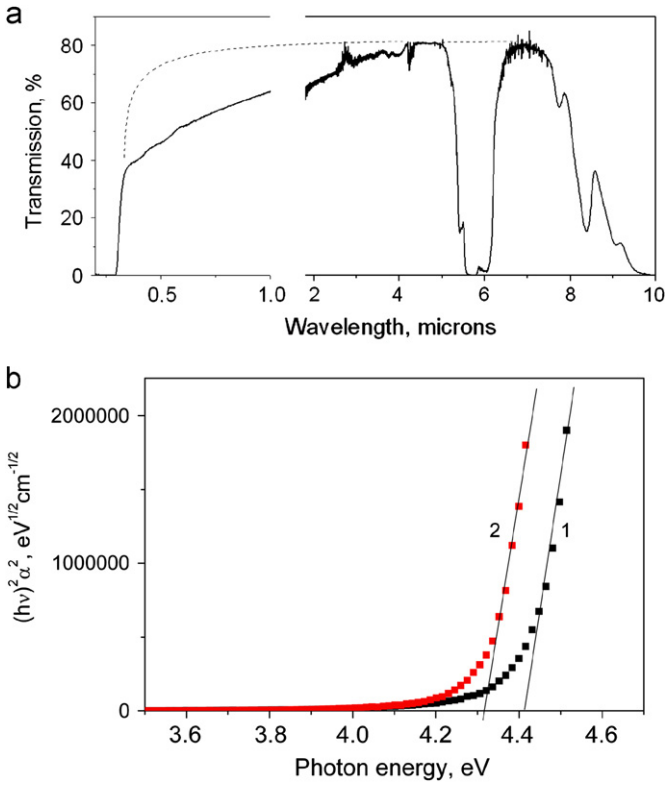

Fig. 3. (a) Transmission spectrum of 1.8 mm thick $K_3WO_3F_3$ single crystal, at $T = 300$ K. Dotted curve shows an expected transmission spectrum in inclusions and water-free $K_3WO_3F_3$. (b) The fundamental absorption edge for 0.3 mm thick $K_3WO_3F_3$ crystal at 80 and 300 K in coordinates $(\alpha h\nu)^2 = f(h\nu)$. Experimental data are given by points whereas solid lines are a result of approximation in the high energy range. Cross points between these lines and abscissa axis gives the bandgap value $E_g = 4.413$ eV ($T = 80$ K) and 4.315 eV (300 K).

Accounting well known phase transitions in $K_3WO_3F_3$ at 415 and 452 K [10,14,17,27] one could expect the drastic changes in the shape and position of the fundamental absorption edge near these transition temperatures. Nevertheless, our careful measurements on the transmission spectra as a function of temperature over the range of 300–500 K disagree this anticipation. In Fig. 4 the dependence of spectral position of a point corresponding to a 20% transmission level on temperature is shown. It is clear that the final curve is smooth enough and there are likely no specific features or kinks related to phase transitions. Namely, it is possible to say that even in the presence of phase transitions in $K_3WO_3F_3$ the spectrum shape and the bangap values change gradually. Experiments with heating of $K_3WO_3F_3$ single crystals in darkness demonstrated the absence of pyroluminescence (defined as a spontaneous emission at heating) in the temperature range from 80 to 600 K. This indicates that no noncentrosymmetric phases with pyroelectric properties appear/disappear over the temperature range [43]. However, the presence of noncentrosymmetric phase without pyroelectric properties, as in the case of $AgGaS_2$ and $AgGaSe_2$, can not be excluded.

The G2-$K_3WO_3F_3$ phase is a polymorph modification with partial O/F ordering and existence of G3-$K_3WO_3F_3$ modification with complete O/F ordering can be reasonably supposed at lower temperatures $T < 300$ K. The stability of Cm phase in $K_3WO_3F_3$ was investigated by DSM-2M microcalorimeter in the temperature range of $T = 300$–110 K. Measurements were carried out in helium atmosphere on the sample with a mass of 0.2 g in heating and cooling modes with a rate of 8 K/min. There was not found

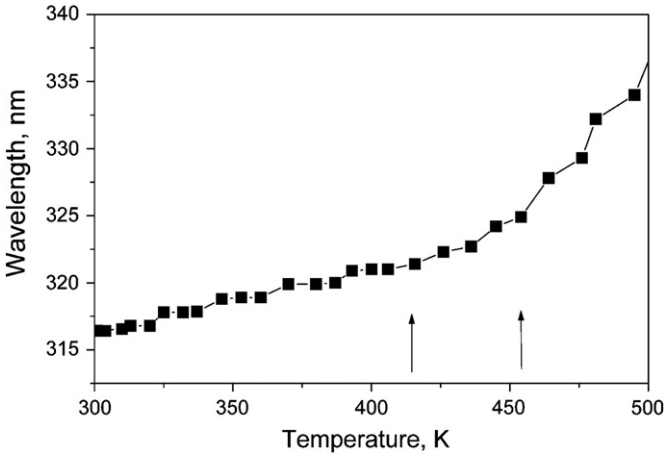

Fig. 4. A smooth shift of fundamental absorption edge (for points with 20% transmission) versus temperature. The arrows show position of phase transitions at 415 and 452 K in $K_3WO_3F_3$.

any anomaly behavior of heat capacity which could be associated with the phase transitions in $K_3WO_3F_3$ below room temperature. This probe indicates that phase transition G2↔G3 may be found at very low temperatures $T < 110$ K if ever occurs.

The calculated electronic structure and the partial density of states (PDOS) for G2-$K_3WO_3F_3$ are shown in Fig. 5(a) and (b). G2-$K_3WO_3F_3$ is predicted as an indirect gap insulator and the direct gap at G point is 0.07 eV larger than the indirect band gap. The calculated energy band gap is 4.2 eV, in good agreement with the experimental value of 4.32 eV. The PDOS analysis clearly shows that the O 2p orbitals are located at the valence band maximum, while the W 5d orbitals are located at the conduction band minimum. They directly determine the band gap. The hybridization between the W 5d and O 2p (and F 2p) orbitals are located in the region from −4 to −7 eV. Compared to the valence band structure measured from XPS (Fig. 6), the good agreement between the calculated and experimental positions for the K 3p, F 2s and O 2s states are achieved if the entire calculated PDOS spectrum is shifted downward by about 5.0 eV. This clearly confirms the validity of the first-principes method. The further comparison reveals that the measured peaks appeared at 5.9 eV and 8.4 eV attribute to the O 2p and W 5d orbitals. It also should be noted that there are no W 4f orbitals appeared in the calculated PDOS, since the f orbitals are not included in the pseudopotential calculations.

Based on the electronic band structures, the refractive indices and second harmonic generation (SHG) coefficients for G2-$K_3WO_3F_3$ are calculated using the formulae in Ref. [44]. At the

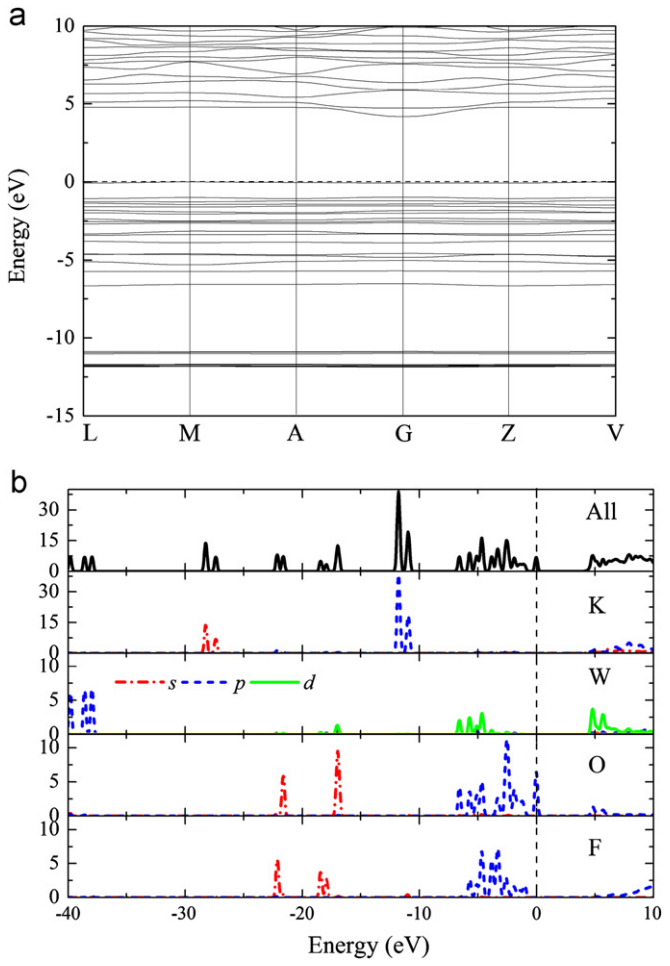

Fig. 5. Electronic properties for the G2-$K_3WO_3F_3$ phase. (a) Band structure along the high symmetry line (b) PDOS projection on the respective orbitals.

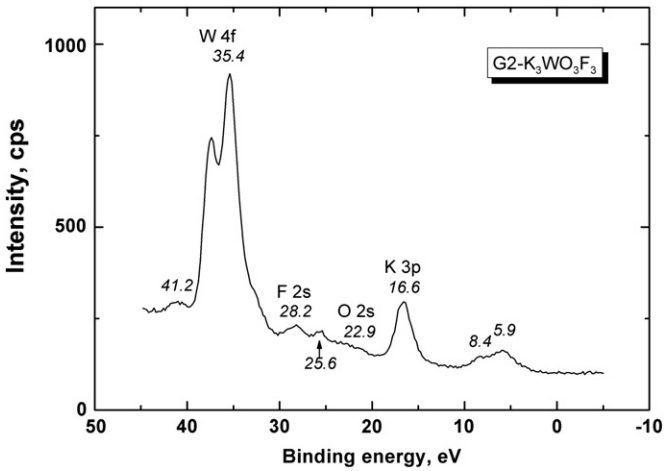

Fig. 6. Valence band states in G2-$K_3WO_3F_3$ as measured with XPS.

Table 2
Nonlinear optical properties of oxyfluoroborates and $K_3WO_3F_3$ (unit: pm/V).

Composition	d_{ij} theo.	Ref.	d_{ij} exp.	Ref.
$KBe_2BO_3F_2$	0.40	[4]	0.49	[1,45]
$RbBe_2(BO_3)F_2$	Not calculated	–	0.45	[2,45]
$CsBe_2BO_3F_2$	Not calculated	–	~0.2	[45]
TlBeBO3F2	Not calculated	–	~0.2	[45]
$BaMgBO_3F$	0.11	[46]	~LBO	[46]
$BaZnBO_3F$	1.24	[46]	≪0.39	[46]
BaCaBO3F	Not calculated	–	0.23	[47]
$BaAlBO_3F_2$	0.74	[48]	1.32	[3]
$Ba_3Sr_4(BO_3)_3$	Not calculated	–	~0.2	[49]
$Ca_5(BO_3)_3F$	Not calculated	–	0.63	[50]
G2-$K_3WO_3F_3$	~3	This study	–	This study

radiation wavelength of 1064 nm, we predict that the refractive indices of G2-$K_3WO_3F_3$ are n_x=1.776, n_y=1.752, n_z=1.741, and the birefringence Δn=0.035. The calculated refractive indices are in reasonable relation with estimation n~1.9 from the above spectroscopic measurements. Moreover, the SHG coefficients are predicted as $d_{11}=-1.97$ pm/V, $d_{31}=0.75$ pm/V, $d_{12}=3.01$ pm/V, $d_{13}=-0.21$ pm/V, $d_{32}=0.70$ pm/V, and $d_{33}=-2.91$ pm/V. Therefore, this crystal has relatively large nonlinear optical coefficients and may achieve the phase-matching condition, the requirement of the effective coherent laser output by harmonic generation, in the mid-IR spectral region. A comparison of nonlinear optical properties of several known fluoroborates and G2-$K_3WO_3F_3$ shown in Table 2 reveals that the oxyfluorotungstates could be the nonlinear optical materials with good performance. A second-harmonic generation (SHG) test was performed by powder method under nanosecond pulse pumping at λ=1.06 μm for the G2-$K_3WO_3F_3$ powder sample prepared by low-temperature chemical synthesis. However, noticeable SHG signal was not detected supposedly due to phase-matching absence at this wavelength and mesostructure developed in the powder sample [15]. The SHG tests on the G2-$K_3WO_3F_3$ single crystal will be performed after the sample with bigger size and better optical quality is obtained. Up to now, the powder SHG signals were detected only in the G2-$Na_3MoO_3F_3$ modification where SHG intensity was about 40 times as large as that of α-quartz [18].

5. Conclusions

The results of present study give new insights into nature and properties of low-temperature noncentrosymmetric modifications

of $K_3WO_3F_3$ oxyfluorotungstate. Crystal structure is defined for G0, G1 and G2 phases subsequently formed on cooling from $T > 452$ to $T \sim 300$ K. Complete O/F disorder at anion position is a characteristic of cubic G0 phase. Partial O/F ordering is obtained for G1 and G2 intermediate phases. Last G3 phase with complete O/F ordering is not found at $T > 110$ K. Thus, existence of G3-$K_3WO_3F_3$ modification is not confirmed up to now.

Effective technology developed for crystal growth of low-temperature G2 modification yields crystals suitable for optical measurements. As a result optical transparency range of 0.3–9.4 μm and band gap $E_g = 4.32$ eV were first time defined for G2-$K_3WO_3F_3$ crystal. This indicates that oxyfluorides are transparent in UV spectral range and this chemical class is promising for creation of new UV materials.

DFT calculations reveals that in G2-$K_3WO_3F_3$ the indirect band gap is governed by the O 2p orbitals located at the valence band maximum and the W 5d orbitals located at the conduction band minimum. Reasonable level of nonlinear optical coefficients and comparatively low birefringence are predicted for G2-$K_3WO_3F_3$, space group *Cm*, by model calculations. The results, however, show a possibility of nonlinear optical properties for oxyfluorotungstates.

Acknowledgments

This study is partly supported by SB RAS Project No. 34. ZSL acknowledges the funding support of No. 91022036, 11174297, 2010CB630701, and 2011CB922204 in China. Authors also wish to thank V. D. Fokina for microcaloric measurements.

References

[1] C.T. Chen, et al., Appl. Phys. B 97 (2009) 9.
[2] C.T. Chen, et al., J. Opt. Soc. Am. B 26 (2009) 1519.
[3] Y. Zhou, et al., Opt. Express 17 (2009) 20033.
[4] Z.S. Lin, et al., J. Appl. Phys. 109 (2011) 073721.
[5] G. Pausewang, et al., Z. Anorg. Allg. Chem. 364 (1969) 69.
[6] J. Ravez, J. Phys. III Fr. 7 (1997) 1129.
[7] K.R. Heier, et al., Inorg. Chem. 38 (1999) 762.
[8] M.S. Molokeev, et al., Powder Diffr. 22 (2007) 227.
[9] M.R. Marvel, et al., J. Am. Chem. Soc. 129 (2007) 13963.
[10] V.D. Fokina, et al., Ferroelectrics 347 (2007) 60.
[11] M.R. Marvel, et al., Z. Anorg. Allg. Chem. 635 (2009) 869.
[12] P.A. Maggard, et al., J. Solid State Chem. 175 (2003) 27.
[13] G. Péraudeau, et al., Solid State Commun. 27 (1978) 515.
[14] J. Ravez, et al., Ferroelectrics 26 (1980) 767.
[15] V.V. Atuchin, et al., Chem. Phys. Lett. 493 (2010) 83.
[16] M.S. Molokeev, et al., Phys. Solid State 53 (2011) 834.
[17] G. Peraudeau, et al., Solid State Commun. 27 (1978) 591.
[18] J.P. Chaminade, et al., Mater. Res. Bull. 21 (1986) 1209.
[19] S.C. Abrahams, et al., Acta Crystallogr.. B 37 (1981) 1332.
[20] F.J. Brink, et al., J. Solid State Chem. 174 (2003) 44.
[21] A.A. Udovenko, et al., Acta Crystallogr. B 64 (2008) 305.
[22] I.N. Flerov, et al., Ferroelectrics 346 (2007) 77.
[23] I.N. Flerov, et al., Phys. Solid State 50 (2008) 515.
[24] I.N. Flerov, et al., Crystallogr. Rep. 56 (2011) 9.
[25] Z.G. Ye, et al., Ferroelectrics 124 (1991) 281.
[26] J.M. Chamberlain, et al., Cryst. Growth Des. 10 (2010) 4868.
[27] A.A. Ekimov, et al., Ferroelectrics 401 (2010) 168.
[28] V.V. Atuchin, et al., Solid State Commun. 150 (2010) 2085.
[29] V.V. Atuchin, et al., Cryst. Growth Des. 11 (2011) 2479.
[30] S.V. Mel'nikova, et al., Phys. Solid State 48 (2006) 117.
[31] S.V. Mel'nikova, et al., Phys. Solid State 52 (2010) 2168.
[32] T.S. Moss, Optical Properties of Semiconductors, Butterworth, London, 1961.
[33] A. Le Bail, Powder Diffr. 19 (2004) 249.
[34] M.C. Payne, et al., Rev. Mod. Phys. 64 (1992) 1045.
[35] S.J. Clark, et al., Z. Kristallogr. 220 (2005) 567.
[36] D. Vanderbilt, Phys. Rev. B 41 (1990) 7892.
[37] J.P. Perdew, et al., Phys. Rev. Lett. 77 (1996) 3865.
[38] H.J. Monkhorst, et al., Phys. Rev. B 13 (1976) 5188.
[39] L. Bellaiche, et al., Phys. Rev. B 61 (2000) 7877.
[40] V.F. Kokorina, Glasses for Infrared Optics, CRC Press, Boca Raton, FL, USA, 1996., p. 236.
[41] T.I. Shishelova, et al., Workshop on Spectroscopy. Water in minerals, Akademiya estestvoznaniy, 2010, (in Russian) ISBN 978-5-91327-093-1.
[42] J. Aarik, et al., Thin Solid films 466 (2004) 41.
[43] A.P. Yelisseyev, et al., Avtometriya 4 (1988) 112. in Russian.
[44] C.T. Chen, et al., Appl. Phys. B 80 (2005) 1.
[45] C.D. McMillen, et al., J. Cryst. Growth 310 (2008) 2033.
[46] R.K. Li, et al., Inorg. Chem. 49 (2010) 1561.
[47] X. Wang, et al., Opt. Mater. 29 (2007) 1658.
[48] H. Huang, et al., J. Appl. Phys. 106 (2009) 103107.
[49] G.C. Zhang, et al., Cryst. Growth Des. 9 (2009) 3137.
[50] K. Xu, et al., Opt. Express 16 (2008) 17735.